Simulation of discontinuous dynamic recrystallization in pure Cu using a probabilistic cellular automaton

Hallberg, Håkan; Wallin, Mathias; Ristinmaa, Matti

Published in:
Computational Materials Science

DOI:
10.1016/j.commatsci.2010.04.012

2010

Computational Materials Science 2010, 49(25-34)

Simulation of discontinuous dynamic recrystallization in pure Cu using a probabilistic cellular automaton

Håkan Hallberg*, Mathias Wallin, Matti Ristinmaa
Division of Solid Mechanics
Lund University, Box 118, S-221 00 Lund, Sweden
*hakan.hallberg@solid.lth.se

Abstract

A cellular automaton algorithm with probabilistic cell switches is employed in the simulation of dynamic discontinuous recrystallization. Recrystallization kinetics are formulated on a microlevel where, once nucleated, new grains grow under the driving pressure available from the competing processes of stored energy minimization and boundary energy reduction. Simulations of the microstructural changes in pure Cu under hot compression are performed where the influence of different thermal conditions are studied. The model is shown to capture both the microstructural evolution in terms of grain size and grain shape changes and also the macroscopic flow stress behavior of the material. The latter gives the expected transition from single- to multiple-peak serrated flow with increasing temperature. Further, the effects on macroscopic flow stress by varying the initial grain size is analyzed and the model is found to replicate the shift towards more serrated flow as the initial grain size is reduced. Conversely, the flow stress is stabilized by larger initial grain sizes. The extent of recrystallization as obtained from simulations are compared to classical JMAK theory and proper agreement with theory is established. In addition, by tracing the strain state during the simulations, a post-processing step is devised to obtain the macroscopic deformation of the cellular automaton domain, giving the expected deformation of the equiaxed recrystallized grains due to the macroscopic compression.

Keywords: Recrystallization, Cellular automaton, Hot compression, Copper

1 Introduction

Parameters such as temperature and strain rate have a major impact on the microstructural evolution during thermomechanical processing of metallic materials. Together with

DOI: 10.1016/j.commatsci.2010.04.012

knowledge of the initial microstructure, these parameters provide tools to control several properties of the final product. An important aspect of the material microstructure is the grain size, control of which allows beneficial combinations of e.g. strength and ductility to be obtained. One of the main metallurgical processes controlling the grain size is dynamic recrystallization, frequently observed in metals during hot working. The recrystallization is driven by a lowering of the Gibbs energy. This may occur either by continuous recovery processes through annihilation and rearrangement of dislocations or by a discontinuous formation of new, relatively dislocation-free, grains through recrystallization. Nucleation of new grains predominantly occur at pre-existing grain boundaries at sites of sufficient stored energy. The recrystallization then proceeds through the migration of high-angle grain boundaries, normally taken as boundaries with a relative misorientation greater than 10-15°. Recovery, on the other hand, occurs by e.g. annihilation of dislocations through cross-slip and climb and arrangement of dislocations in low-angle (2-5°) subgrain boundaries. In materials of low stacking-fault energy, such as copper, the dynamic recovery is slow in favor of dynamic discontinuous recrystallization. In contrast, high stacking-fault energy materials such as aluminum exhibit rapid dynamic recovery which makes continuous dynamic recrystallization the dominating mechanism for the formation of new grains. After the initial formation of recrystallized grains, subsequent grain growth occurs due to migration of grain boundaries, however also driven by a reduction of the total grain boundary area in the microstructure, cf. [1].

Materials undergoing dynamic recrystallization are characterized by an initially serrated flow curve, exhibiting either cyclic or single peak oscillations. At lower temperatures and higher strain-rates, the tendency is towards single peak flow, while elevated temperatures and lowered strain-rates promote multiple-peak flow behavior, [2, 3, 4, 5]. This is often explained as an effect of the competitive processes of work hardening and softening due to recrystallization, i.e. between dislocation generation by deformation and dislocation annihilation by recrystallization. At low strain rates, most of the microstructure is recrystallized before the regions that were first to be recrystallized have deformation hardened enough to initiate a new cycle of recrystallization. If the strain rate is increased, multiple recrystallization cycles may occur in parallel, damping out the flow curve oscillations, cf. [2, 4, 6].

Cellular automata have become a widely used tool in materials science for simulating microstructural evolution in terms of e.g. phase transformation, solid state precipitation, dendrite growth during solidification of melts, spherulite growth in polymers and recrystallization. Cellular automata modeling of – primarily static – recrystallization has been studied by several authors, e.g. [7, 8, 9, 10, 11, 12].

In the present work, a cellular automaton with probabilistic cell state switching rules is employed in the simulation of microstructural evolution in pure Cu under hot-working conditions. The effects of different temperatures are studied and compared to experimental

findings in the literature. A description of the grain boundary energy, valid for the entire range of misorientation angles in contrast to the commonly used Read-Shockley relation, is an important aspect of the present model. Further, a viable incremental algorithm for the grain growth kinetics is obtained by tuning of the numerical model to analytical expressions. Deformation of the analysis domain is obtained by identifying the strain state throughout the simulations. In addition to these model features, it can be noted that the grain boundary driving pressure is a result of the competing processes of stored energy minimization and grain boundary area reduction.

This paper is divided into sections, beginning with a description of the recrystallization kinematics and the governing equations for nucleation and growth of recrystallized grains. That section is followed by a description of the cellular automaton formulation employed in the current work, its switching rules and updating scheme. The subsequent sections presents material parameter calibration followed by a presentation of results compared to experimental data together with a discussion on the findings. Some finishing remarks closes the paper.

2 Evolution laws and recrystallization kinematics

During inelastic deformation dislocations will be generated, resulting in increasing stored energy. If recovery by dislocation annihilation is slow as in materials of low stacking-fault energy, grain nuclei may start to form. The nucleation predominantly occurs along grain boundaries, cf. [4, 13], although additional sites such as at shear bands and near particle inclusions, causing strong lattice curvature, also contributes. The nucleation of new grains is in this way a manifestation of a thermodynamically unstable material microstructure, cf. [1]. In combination with recovery, the microstructure may reach a thermodynamically more favorable state by growth of new, relatively dislocation-free, grains from the nuclei. The dislocation density ρ in a grain, with diameter d, is assumed to evolve according to a Kocks-Mecking relation, cf. [14, 15, 16, 17], i.e.

$$\dot{\rho} = \left(k_1 \sqrt{\rho} - k_2 \rho + \frac{1}{bd} \right) \dot{\varepsilon}^{\mathrm{p}}_{\mathrm{eff}} \tag{1}$$

where $k_{1,2}$ are parameters and b is the magnitude of the Burgers vector. Note that a superposed dot denotes differentiation with respect to time. The rate of the effective plastic strain is denoted by $\dot{\varepsilon}^{\mathrm{p}}_{\mathrm{eff}}$.

In the present model, the rate of nucleation per unit of grain boundary area is taken as

$$\dot{N} = c \dot{\varepsilon}^{\mathrm{p}}_{\mathrm{eff}} \exp\left(-\frac{Q_{\mathrm{n}}}{RT} \right) \tag{2}$$

where T is the absolute temperature, c a constant, R the gas constant and Q_{n} the activation energy for nucleation. This corresponds to the proportional nucleation model of [18, 19]

which has also been used by e.g. [20, 21, 22]. The nucleation activation energy in (2) is for simplicity taken as a constant parameter in the present model whereas this quantity is likely to depend on the state of the microstructure at a given location, e.g. in terms of the local stored energy. As discussed previously, nucleation predominantly occur along grain boundaries at sites where sufficient stored energy is present. Following [23], this process is viewed as a bulging of the grain boundary upon reaching the critical dislocation density needed for the nucleation to be initiated. Following the arguments of [6], the critical dislocation density for nucleation to occur at a boundary site is given by

$$\rho_{\mathrm{c}} = \left(\frac{20\gamma\dot{\varepsilon}^{\mathrm{p}}_{\mathrm{eff}}}{3blM\tau^2} \right)^{1/3} \tag{3}$$

where $\tau = \mu b^2/2$ is the dislocation line energy and where γ is the grain boundary energy, defined below. The dislocation mean free path l, appearing in (3) is for simplicity taken as the average distance between dislocations, giving $l = \rho^{-1/2}$.

The dynamic recrystallization is not initiated until a certain strain has been reached in the grains. This critical strain is denoted by ε_{c} and correspond to the critical strain at nucleation initiation as discussed by e.g. [2, 6]. Nucleation of new grains – i.e. the initiation of recrystallization – is in this way delayed until $\varepsilon^{\mathrm{p}}_{\mathrm{eff}} \geq \varepsilon_{\mathrm{c}}$, where the threshold strain ε_{c} is determined by calibration against experimental data for different temperatures, as shown below. By the introduction of a critical strain, we follow the common approach for determination of the onset of recrystallization. Threshold values for recrystallization initiation have in this way been used previously by e.g. [22, 24, 25] and is further discussed by [26]. The use of a critical strain allows convenient identification of the point of recrystallization initiation when considering experimental data. This is further discussed below in relation to the calibration of the model.

The grain boundary migration velocity is directed along the local grain boundary normal and the velocity magnitude is given by

$$v = MP \tag{4}$$

where M is the grain boundary mobility and P the pressure available to drive the grain boundary motion. Such recrystallization and grain growth kinetics were addressed already by [27] where the migration of grain boundaries under the influence of a driving force was studied. For the sake of simplicity, the grain boundary mobility M is in the present model assumed to be a function of temperature, identical for all boundaries in the microstructure. As mentioned, grain growth is driven by a lowering of the stored energy which can be written as $\tau\rho$. Assuming spherical grains, cf. [23, 28], the total energy related to a grain of radius r can be described by a surface energy term, W^{surf}, and a volumetric energy term, W^{vol}. The volumetric energy stems from the jump in dislocation density $[\rho]$ across the

boundary. The potential function for the grain boundary driving force can now be written as

$$W = W^{\mathrm{vol}} + W^{\mathrm{surf}} \quad \text{where} \quad W^{\mathrm{vol}} = \frac{4}{3}\pi r^3 \tau[\rho] \quad \text{and} \quad W^{\mathrm{surf}} = 4\pi r^2 \gamma \tag{5}$$

The volumetric term is considered in the models of [29, 30] while the boundary energy term is used in the models of [22, 31]. Using (5), the driving force F for grain boundary migration will be related to the energy change occurring as the size of the grain is changed, i.e.

$$F = \frac{dW}{dr} = 4\pi r^2 \tau[\rho] - 8\pi r\gamma \tag{6}$$

Next, the driving pressure acting on the boundary is obtained by dividing the driving force by the boundary area of the spherical grain, giving

$$P = \tau[\rho] - \frac{2\gamma}{r} \tag{7}$$

Note that the grain boundary energy term in (7) is dependent on the grain radius r, i.e. the local curvature of the grain boundary. The curvature calculation is considered later on, in relation to the formulation of the cellular automaton algorithm. The grain boundary energy, γ, first appearing in (5), is related to the relative misorientation θ between adjacent grains. For low-angle grain boundaries with θ less than approximately 15°, the grain boundary energy is often assumed to follow the Read-Shockley relation, cf. [4, 32]. The Read-Shockley relation is in its original form, however, valid only for small misorientation angles. A more appealing approach is to use the modified Read-Shockley model by [33], also employed by e.g. [34], which reads

$$\gamma = \gamma_{\mathrm{m}} \sin(2\theta) \left\{1 - r_\gamma \ln\left[\sin(2\theta)\right]\right\}, \quad 0 \leq \theta \leq 90^\circ \tag{8}$$

where γ_{m} and r_γ are constants, specified below in relation to the calibration of the model. The format in (8) is adopted in the present model.

The mobility of the grain boundaries is described through the Turnbull estimate, cf. [35], and can be written as

$$M(T) = M_0(T) \exp\left(-\frac{Q_{\mathrm{m}}}{RT}\right) \tag{9}$$

where Q_{m} is the activation energy for boundary migration. The mobility laws used by e.g. [4, 8, 9, 11, 22, 28, 30, 36] are obtained from (9) by choosing different forms of the pre-exponential term M_0. This quantity is further considered during the calibration of the model. The recrystallization process may now be described by nucleation according to (2) and subsequent growth by (4), with driving pressure and boundary mobility given by (7), (8) and (9).

3 Cellular automaton formulation

A representative volume element of dimensions 200×200 microns is discretized using 46800 hexagonal cells with typical cell dimension l_c, cf. Fig. 2. Each cell is interacting with its closest neighbors and is characterized by four state variables: the orientation, the dislocation density, the status (pre-existing grain or recrystallized grain) and an identifier (which grain number the cell belongs to). An initial microstructure is generated with a chosen number of grains by allowing a fixed number of nuclei to grow until they impinge upon each other, cf. Fig. 1. The number of grains and the dimensions of the cellular automaton are chosen to obtain a certain initial average grain size. Next, the grains are given a random initial dislocation density taken from a normal distribution with mean 10^{11} m^{-2} and standard deviation 10^{10} m^{-2}, representative for the annealed state, cf. [37]. The dislocation density is for simplicity assumed to be homogeneously distributed within each grain. In addition to the dislocation density, the grains of the undeformed microstructure are also given a random initial orientation from a uniform distribution in the interval between 0 and 90°, resulting in an isotropic orientation distribution.

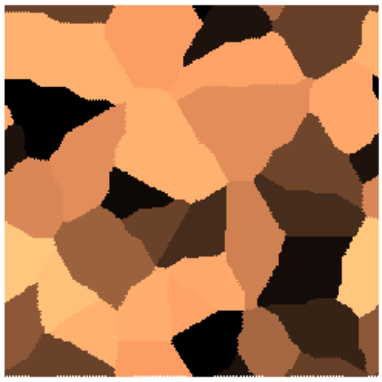

Figure 1: The initial microstructure used in the simulations. The size of the analysis domain is 200×200 microns. The colors are randomly set in order to distinguish between the different grains.

Recalling (4), it was found that the surface energy term is dependent on the curvature r of the grain boundary. In the present work the local grain boundary curvature is obtained from an expanded neighbor region, including the first-, second- and third-nearest cell neighbors. The local grain boundary radius is found by evaluating

$$r = a_r \frac{n+1}{n_k - n_i} \tag{10}$$

where a_r is a coefficient further discussed in the following, $n = 36$ is the total number of neighbor cells, n_i is the number of neighbors within the current neighborhood that belongs

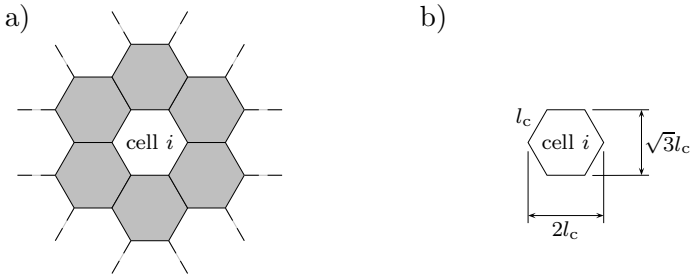

Figure 2: The definition of a hexagonal cell i in the cellular automata grid. (a) Nearest-neighbor area of influence (shaded gray). (b) Geometrical definition of a cell with side length l_c.

to the grain and $n_k = 18$ is the number of neighbors belonging to the grain in the case of a locally planar boundary. Note that for a locally planar boundary, $n_k = n_i$ and $r \to \infty$ is obtained. A local curvature estimate on the form (10) was first introduced by [38] and has since been used also by e.g. [22, 39].

To obtain an estimate for the average grain size in the microstructure under consideration, average sizes for each grain are needed. Following [40], the 2D microstructure is viewed as a cross-section of a corresponding 3D microstructure, allowing the average radius of a grain to be obtained as

$$\bar{r} = \sqrt{\frac{n_c A_c}{\pi}} \tag{11}$$

where n_c is the number of cells belonging to the grain and where $A_c = \frac{3\sqrt{3}}{2} l_c^2$ is the area of one cell, cf. Fig. 2.

Once the critical strain ε_c is reached, the number of new nuclei to appear is obtained by integration of the nucleation rate equation (2), giving $\Delta N = \dot{N} \Delta t$. Possible nucleation sites are then obtained by considering all grain boundary cells pair-wise across the boundaries. If the average dislocation density of the two cells is $\geq \rho_c$, this is a viable nucleation site. All possible nucleation sites are then given a probability $w_{\text{nucl.}}$ for nucleation where the possible nucleation site with the highest stored energy receives the nucleation probability 1. Effectively, the ratio between the local and the maximum dislocation densities among the possible nucleation sites is evaluated according to

$$w_{\text{nucl.}} = \frac{\rho_{\text{local}}}{\rho_{\text{max}}} \quad \text{where} \quad \rho_{\text{local}} \leq \rho_{\text{max}} \tag{12}$$

Going through the possible nucleation sites, a random number $\xi \in [0, 1]$ is generated and compared to the nucleation probability of the current site. If $\xi \leq w_{\text{nucl.}}$ the nucleus is placed

at the site and if $\xi > w_{\text{nucl.}}$, the site is rejected. This is done until all nuclei appearing in the current step have been placed. Each new nucleus is given the average orientation of the two boundary cells involved, cf. [41], and zero dislocation density. A zero initial dislocation density is here chosen for simplicity although it is noted from e.g. [42] that the new grains are not entirely free of dislocations.

After the nucleation step, growth of the recrystallized grains is considered. The grain boundaries in the microstructure will have different local migration rates due to variations in driving force and boundary mobility. Since the cell size of the cellular automaton is fixed it appears unphysical that all moving boundaries are able to switch the status of neighboring cells during one time step. In the present work the approach used by e.g. [11] is adopted, where a probabilistic switching condition is employed. The local switching probability w_{growth} is taken as the ratio between the velocities of the local grain boundary and the fastest moving grain boundary in the cellular automaton. The cell switching probability is thus calculated as

$$w_{\text{growth}} = \frac{v_{\text{local}}}{v_{\text{max}}} \quad \text{where} \quad v_{\text{local}} \leq v_{\text{max}} \tag{13}$$

In each step, and for each cell, a random number $\xi \in [0, 1]$ is again generated. If $\xi \leq w_{\text{growth}}$ the switch is accepted and if $\xi > w_{\text{growth}}$ it is rejected. This approach allows a synchronous update of the cells. If a cell has two or more growing, recrystallized, neighbors, the neighbor with the highest grain boundary velocity will be the one to possibly consume the current cell. Since the driving force for boundary migration is based on the difference in stored energy, this selection rule gives the greatest reduction in the stored energy of the system. Recrystallized grains will continue to grow until the driving force becomes zero. The evolution of the dislocation densities in the grains is considered in each time step by evaluating (1) and using the current time increment, i.e.

$$\Delta\rho = \left(k_1\sqrt{\rho} - k_2\rho + \frac{1}{bd} \right) \Delta\varepsilon^{\text{p}}_{\text{eff}} \tag{14}$$

By noting that for given dislocation densities and given orientations, an analytical expression for the growth velocity of a grain can be obtained from equations (4), (7) and (9). In order to study the growth of such an analytical grain, the parameter choices $k_1 = 7.3 \times 8$ m^{-1}, $k_2 = 24.1$, $\mu = 30$ GPa, $b = 0.256$ nm, $\gamma_{\text{m}} = 0.625$ J·m^{-2} and $r_\gamma = 0.66$ are made, corresponding to pure copper at 725 K. The initial difference in dislocation density across the boundary is set to $[\rho] = 1 \times 14$ m^{-2} and the misorientation is taken as $\theta = 45°$. This procedure allows tuning of the cellular automaton algorithm to the analytical exact solution in terms of the timestep Δt_{c}, the reference boundary velocity v_{c} and the parameter a_{r}, appearing in the local radius estimation (10). By choosing the values $\Delta t_{\text{c}} = 0.465$ s, $v_{\text{c}} = 4.3$ μm/s and $a_{\text{r}} = 2$ μm, a comparison between the growth of an

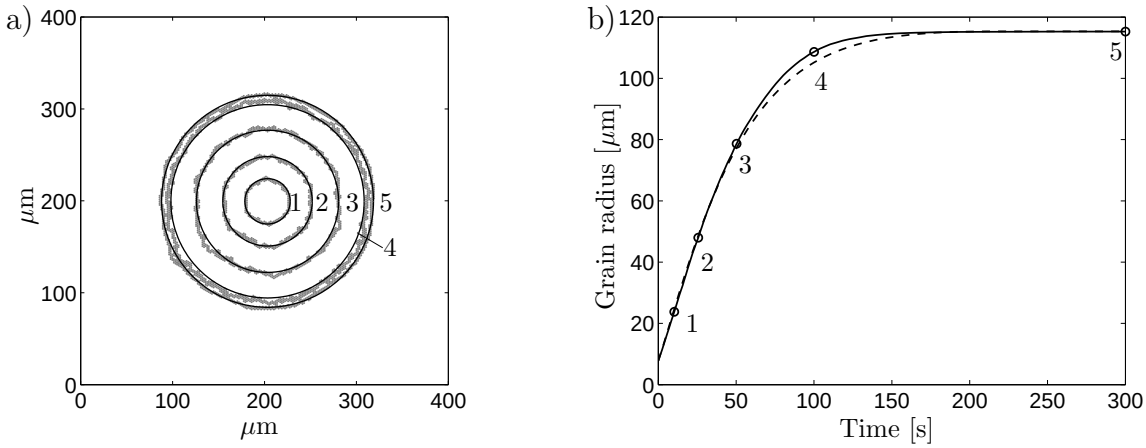

Figure 3: (a) Comparison of the sizes of a cellular automaton grain (shaded gray) and an analytical grain (solid line). The numbers correspond to the points indicated in the figure to the right. The square frame shows the boundaries of the cellular automaton. (b) Radii of the cellular automaton grain (solid line) and an analytical grain (dashed line) as functions of time.

analytical grain and a cellular automaton grain is obtained as shown in Fig. 3. Next, when performing analyses using a polycrystalline cellular automaton, the timestep Δt is obtained by scaling the maximum occurring grain boundary velocity $v_{\max}$ with the tuned growth distance $\lambda_{\mathrm{c}} = v_{\mathrm{c}}\Delta t_{\mathrm{c}}$ by setting $\Delta t = \lambda_{\mathrm{c}}/v_{\max}$. The current cellular automaton algorithm is summarized as a pseudo-code in Box 1.

Considering a representative volume element, consisting of several grains, the flow stress related to the average dislocation density, $\bar{\rho}$, is classically described by

$$\sigma = \alpha\mu b\sqrt{\bar{\rho}} \tag{15}$$

where α is a parameter related to the strength of the dislocation interactions, cf. [43], and μ is the shear modulus. To obtain the average dislocation density a homogenization of the plastic power $\dot{w}^{\mathrm{p}}$ is considered, i.e.

$$\dot{w}^{\mathrm{p}} = \sigma\dot{\varepsilon}^{\mathrm{p}}_{\mathrm{eff}} = \frac{1}{V}\sum_i \int_{V_i} \dot{w}^p_i dV = \frac{1}{V}\sum_i \int_{V_i} \sigma_i \dot{\varepsilon}^{\mathrm{p}}_{\mathrm{eff},i} dV \tag{16}$$

where a subscript i denotes quantities related to grain i and where V is the total volume of the representative volume element under consideration. Using $\sigma_i = \alpha\mu b\sqrt{\rho_i}$ and $\dot{\varepsilon}^{\mathrm{p}}_{\mathrm{eff}} = \dot{\varepsilon}^{\mathrm{p}}_{\mathrm{eff},i}$ results in

$$\sqrt{\bar{\rho}} = \frac{1}{V}\sum_i \int_{V_i} \sqrt{\rho_i} dV \tag{17}$$

Note that in (16) and (17), summation is performed over all grains.

Box 1 The cellular automaton algorithm used for the present model.

Generate the initial microstructure

Establish global conditions: T, M, $\dot{\varepsilon}^{\mathrm{p}}_{\mathrm{eff}}$, λ_{c} and final strain $\varepsilon^{\mathrm{p}}_{\mathrm{eff,final}}$

Calculate the maximum possible boundary velocity $v_{\max}$ in the initial microstructure

while $\varepsilon^{\mathrm{p}}_{\mathrm{eff}} < \varepsilon^{\mathrm{p}}_{\mathrm{eff,final}}$

Calculate the timestep $\Delta t = \lambda_{\mathrm{c}}/v_{\max}$

Calculate the increment in effective plastic strain: $\Delta\varepsilon^{\mathrm{p}}_{\mathrm{eff}} = \dot{\varepsilon}^{\mathrm{p}}_{\mathrm{eff}}\Delta t$

if $\varepsilon^{\mathrm{p}}_{\mathrm{eff}} > \varepsilon_{\mathrm{c}}$

Calculate the increase in number of nuclei $\Delta N = \dot{N}\Delta t$

Find all possible nucleation sites by using (3)

Obtain a random number $\xi \in [0, 1]$

Distribute grain nuclei according to the probability condition (12)

for each cell

- Calculate the local boundary radius r from (10)
- Calculate the local grain boundary energy γ from (8)
- Calculate the driving pressure P from (7)
- Calculate the local boundary velocity v_{local} according to (4)
- Calculate a random number $\xi \in [0, 1]$
- Calculate the new cell state according to the probability switch (13)
- Calculate the updated dislocation density ρ according to (14)

end for

end if

Store the maximum boundary velocity $v_{\max}$ that occurred during the step

Update the state of all cells simultaneously

end while

4 Results

Pure Cu, a low stacking-fault energy material prone to dynamic discontinuous recrystallization, is taken as model material. Beginning with the temperature-dependent shear modulus, first appearing in (15) this quantity is assumed to have a temperature dependence as given by [36], i.e.

$$\mu(T) = 35.4 \times 10^9 \left[1 - 0.5 \left(\frac{T - 300}{T_{\mathrm{m}}}\right)\right] \ \mathrm{Pa} \tag{18}$$

where $T_{\mathrm{m}} = 1356$ K is the melting point temperature. The analysis region is assumed to be crystallographically oriented so that the grain misorientations can be described by [001] tilt boundaries. Data on the dependence of the boundary energy on misorientation for 99.98 %-purity Cu at 1065 K is presented by [44]. Since the material considered here is of higher purity and since the present temperature interval goes below 1065 K, the maximum boundary energy is instead taken as $\gamma_{\mathrm{m}} = 0.625$ J·m^{-2} according to [36]. The boundary energy parameter is, however, set to $r_\gamma = 0.66$ motivated by the appearance of the data in [44]. The resulting boundary energy is shown in Fig. 4. The material parameters used are

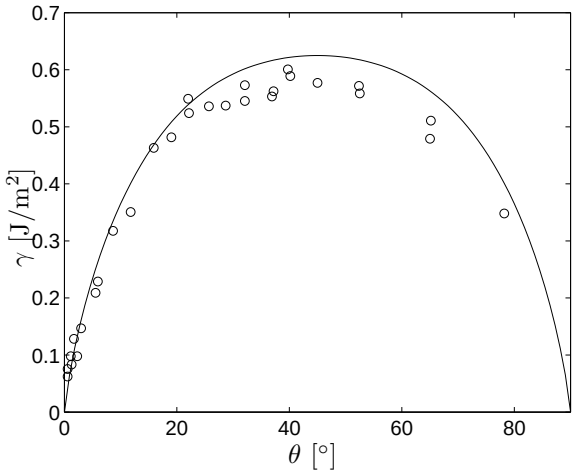

Figure 4: Description of the grain boundary energy (8) for the current 99.99 %-purity Cu (solid line) shown together with experimental data taken from [44] regarding 99.98 %-purity Cu at 1065 K (symbols).

summarized in Table 1. Calibration of the temperature dependent parameters ε_{c}, c, k_1, k_2 and M_0 is conducted using experimental data from hot compression tests, cf. Fig. 5b, giving the temperature dependencies presented in Table 2. Experimental data is taken from [46]. The resulting flow stress curves, obtained from the cellular automaton simulations, are shown i Fig. 5a.

Table 1: Material parameters entering the present model. The values are valid for pure Cu.

Parameter	Value	Description	Source
T_m	1356 K	Melting temperature	[36]
γ_m	0.625 J·m^{-2}	Grain boundary energy	[36]
r_γ	0.66	Grain boundary energy parameter	[44]
α	0.5	Dislocation interaction strength parameter	[22]
Q_m	126 kJ·mol^{-1}	Activation energy for grain boundary migration	[45]
b	0.256 nm	Magnitude of the Burgers vector	[15]
Q_n	261 kJ·mol^{-1}	Activation energy for nucleation	[46]

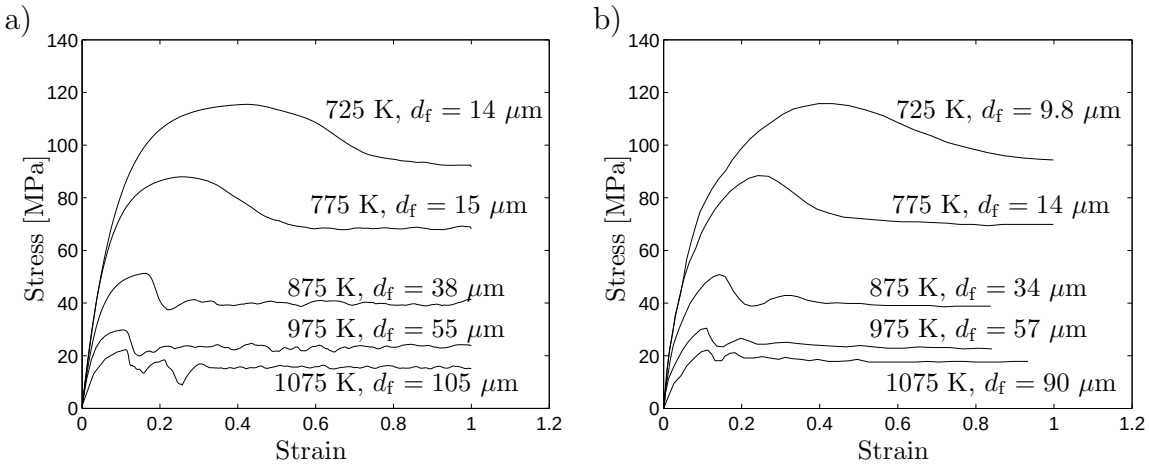

Figure 5: Stress strain response for different constant temperatures. The final grain sizes, d_f, are stated at each temperature. (a) Simulation results obtained using an initial average grain size of 77 μm. (b) Experimental results from hot compression tests presented in [46]. Initial average grain size 78 μm.

Table 2: Temperature dependencies of the critical strain ε_c, the nucleation parameter c, the parameters k_1 and k_2 in the evolution law for the dislocation density and the pre-exponential grain boundary mobility parameter M_0.

T [K]	ε_c	c [m^{-2}]	k_1 [m^{-1}]	k_2	M_0 [m^3·N^{-1}·s^{-1}]
725	0.4	3.5×10^{22}	379.5	1.3×10^{-5}	3.6×10^{-5}
775	0.23	3×10^{21}	405.6	1.7×10^{-5}	3.6×10^{-5}
875	0.15	4×10^{18}	458.0	3.4×10^{-5}	6.4×10^{-5}
975	0.1	8×10^{16}	510.3	6.5×10^{-5}	9.5×10^{-5}
1075	0.1	6.7×10^{15}	562.7	9.3×10^{-5}	1.6×10^{-4}

Since the experimental results used for calibration of the model stem from axisymmetric compression tests, the deformation of the cellular automaton can be obtained to visualize the flattening of the grains due to compression. Denoting the compressive axis by 3 and

the radial and circumferential axes by 1 and 2 allows the total logarithmic strain rates in the different directions to be calculated, under the assumption of von Mises plasticity, as

$$\begin{aligned}\dot{\varepsilon}_1 &= \dot{\varepsilon}_2 = -\nu\frac{\dot{\sigma}}{E} - \frac{1}{2}\frac{\sigma}{|\sigma|}\dot{\varepsilon}^{\mathrm{p}}_{\mathrm{eff}} \\ \dot{\varepsilon}_3 &= \frac{\dot{\sigma}}{E} + \frac{\sigma}{|\sigma|}\dot{\varepsilon}^{\mathrm{p}}_{\mathrm{eff}}\end{aligned} \tag{19}$$

where $\nu = 0.3$ and $E = 110$ GPa is the Poisson ratio and the elastic modulus, respectively. Note that the compressive stress $\sigma_3 = \sigma$, as obtained from (15). The results in (19) allow a post-processing step to be performed on the cellular automaton results where the deformation is imposed on the analysis domain.

With the initial microstructure shown in Fig. 1, the evolution of grain size and grain shape with increasing strain is shown in Fig. 8. Nucleation of new grains occur at the grain boundaries present in the microstructure. If there is a large difference in the sizes of the previously existing grains and the newly recrystallized grains there is a tendency for formation of so-called necklace patterns of recrystallized grains along the boundaries of the pre-existing grains. In contrast, if the relative size difference between old and new grains is smaller, there is less tendency for necklace formation, cf. [4, 42, 47]. It can be noted that at the lower temperatures of 725 K and 775 K, there is a tendency for necklace patterns of new grains along the pre-existing grain boundaries. Moving up in temperature, this tendency is weakened. At these higher temperatures, larger recrystallized grains are growing, consuming the previous grain boundaries before a clear necklace pattern can form. The recrystallization is thus more rapid at higher temperatures, not allowing one cycle of recrystallization to finish before the next one is initiated. This results in the oscillations of the flow stress curves, shown in Fig. 5, at higher temperatures. At the lower temperatures of 725 K and 775 K, each cycle of recrystallization is allowed be completed – or at least nearly completed – before the next one sets in, resulting in more stable flow stress behavior.

The recrystallization kinetics during experimental analysis is often studied according to the Johnson-Mehl-Avrami-Kolmogorov (JMAK) theory using the Avrami equation, cf. [48, 49, 50], which can be formulated as

$$X = 1 - \exp\left(-Bt^n\right) \tag{20}$$

where X is the recrystallized volume fraction and t is the time. In the present simulations, X is taken as the recrystallized area fraction since the two-dimensional analysis region is viewed as a cross-section of a corresponding three-dimensional domain. The simulated volume fraction of recrystallized material is illustrated in Fig. 6a. The two parameters B and n in (20) are determined from a double-logarithmic Avrami plot of the experimentally measured extent of recrystallization as a function of time. The n-parameter corresponds to the slope of the linear Avrami plot and the B-parameter is related to the nucleation rate

and grain boundary kinetics of the microstructure under consideration, cf. [7, 10, 18, 51]. The Avrami model (20) was formulated under the assumptions of site-saturated and homogeneous nucleation with constant grain boundary velocity. Results from experiments where heterogeneous and non-constant grain boundary velocity comes into play deviates, however, from the linear appearance of the theoretical Avrami plot, cf. [7, 10]. This occurs at the initial stages where the assumption of site-saturated nucleation is least applicable and at the last stages of recrystallization where growing grains to a large extent has consumed possible nucleation sites. For a constant nucleation rate, which is the case in the present model at constant temperature, experimental results predict a value of $n = 3$ for two-dimensional grain growth while $n = 2$ correspond to two-dimensional, site-saturated, nucleation, cf. [10]. Considering the nucleation parameter c, specified in Table 2, it can be noted that by moving down in temperature, the value of c increases. High values of c will lead to full population of all possible nucleation sites at all stages of the recrystallization process, i.e. site-saturated nucleation. This trend from almost site-saturated towards a more heterogeneous, but still constant, nucleation rate with increasing temperature is seen in Fig. 6b where the simulated recrystallized fraction is fitted with the Avrami function (20). As the temperature is increased – i.e. as the nucleation becomes more heterogeneous – the value of n shifts from $n = 2$ for 725 K and 775 K to $n = 3$ at 875 K and 975 K, in accordance with the findings in [10].

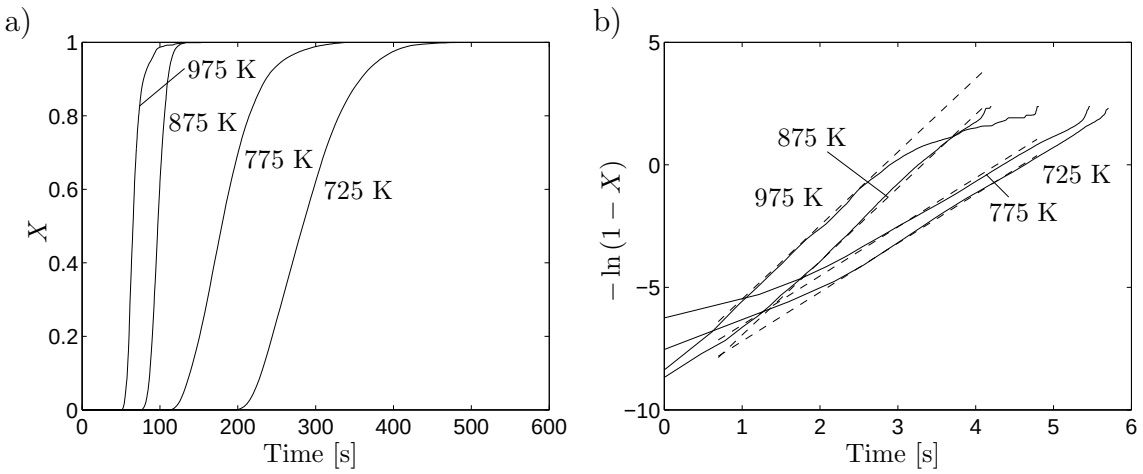

Figure 6: (a) Recrystallized volume fraction obtained from simulations at different temperatures. (b) Avrami plot of the recrystallized volume fraction. Simulation results (solid lines) from the present model are fitted with the theoretical model (dashed lines) given by (20). Note that logarithmic axes are used in (b).

The effect of varying the initial grain size is illustrated in Fig. 7. As the initial grain size is reduced, flow stress oscillations appear while an increased initial grain size stabilizes

the flow stress behavior. The simulations replicate the experimentally obtained behavior as presented by [46], cf. Fig. 7b. A decreased initial grain size could be the result of e.g. changed heat-treatment conditions prior to the forming process. As the initial grain size is refined the volume fraction of grain boundary area – and thus the number of possible nucleation sites for recrystallization – increases. This allows repeated and simultaneous cycles of recrystallization to take place, giving increasing flow stress serrations. In contrast, an increased initial grain size reduces the number of possible nucleation sites and slows down the recrystallization process. As shown in Fig. 5, the final grain size at some of the

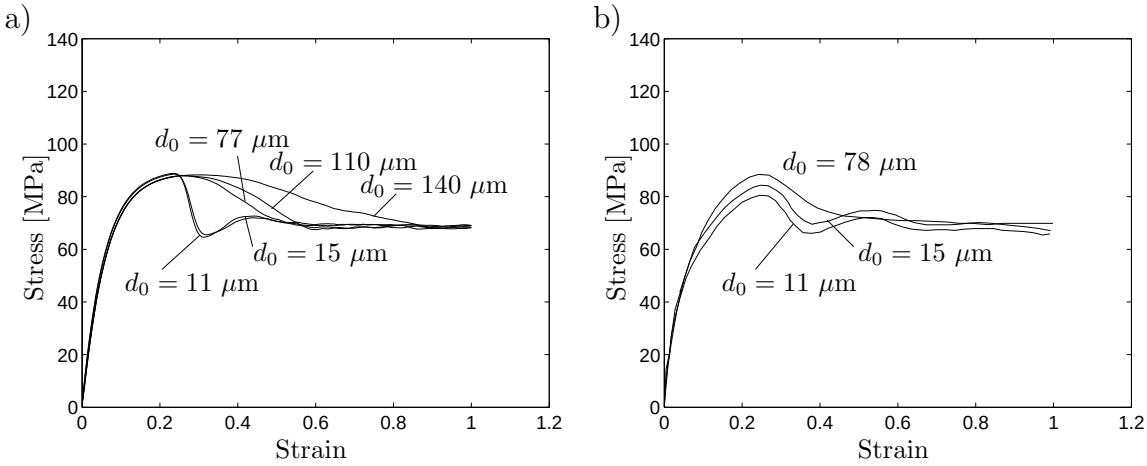

Figure 7: Stress strain response at 775 K for three different initial average grain sizes d_0. (a) Simulation results. (b) Experimental results from hot compression tests presented in [46].

considered temperatures deviates slightly from the experimental values. This could in part be explained by the assumption of spherical grains in the simulations and in part by the nucleation which in the model only occur at grain boundaries, while additional nucleation sites in the grain interiors, e.g. at inclusions, could also be present in reality. In Fig. 5, the flow stress corresponding to 1075 K, the highest of the considered temperatures, exhibit some excessive serrations initially. This is due to the chosen cellular automaton size of 200×200 microns which might be inadequately small in comparison to the grain size of approximately 100 microns, present at this temperature. Fig. 8 also illustrate the tendency for formation of equiaxed grains with progressing recrystallization, rendering more regular grain shapes throughout the microstructure at larger strains. This is especially the case at the lower of the considered temperatures. The development of a more regular, equiaxed, microstructure with a relatively constant mean grain size with progressing deformation is also discussed in relation to experiments by e.g. [2]. The compressive deformation imposed onto the workpiece using (19), of course result in the equiaxed grains becoming elongated

perpendicular to the compressive axis as seen in Fig. 8.

The evolution of the average grain size at different temperatures is shown in Fig. 9. It can be noted that the rapid and over-lapping cycles of recrystallization at the lower of the studied temperatures result in more distinct grain size distributions. The states of effective plastic strain $\varepsilon^{\mathrm{p}}_{\mathrm{eff}} = 0$, 0.5 and 1 correspond to the microstructures shown in Fig. 8.

5 Conclusions

In materials of low stacking-fault energy, stored energy release due to dislocation annihilation processes such as cross-slip and climb is slow in favor of dynamic recrystallization. The material undergoing this type of microstructural change is characterized by nucleation of grain embryos at the grain boundaries and subsequent growth of equiaxed grains. If the process is allowed to proceed, a steady-state grain size is obtained with increasing macroscopic plastic deformation. The changes in material behavior by softening due to recrystallization and competing deformation hardening is reflected in the appearance of the macroscopic flow stress. Under thermomechanical processing characterized by relatively lower temperatures and higher strain-rates, single-peak flow is observed while further elevated temperatures and lowered strain rates promote serrated multiple-peak flow. The effects of temperature and strain rate on the flow stress behavior is further influenced by the grain size in the initial microstructure. Keeping temperature and strain rate fixed, changes in the initial grain size may cause transitions between single- and multiple-peak flow.

The present model of dynamic recrystallization builds on evolution laws and recrystallization kinetics formulated on the microlevel. Driven by the effective plastic strain, the dislocation density evolves under an interplay between dislocation generation and annihilation. The extent of recrystallization is proportional to the level of plastic deformation exerted onto the material, motivating an expression for the nucleation rate of new grains that is proportional to the rate of plastic deformation. Grain growth is described by the competing processes of stored energy minimization and grain boundary area reduction. This leads to an analytical expression for the local grain boundary velocity in the microstructure. Grain boundary energy is calculated by means of a modified Read-Shockley formulation, valid in the entire range of misorientations. The recrystallization model is employed in a cellular automaton algorithm with probabilistic cell updating switches, allowing simulation of both the spatial and temporal microstructural changes in a representative volume element under hot deformation conditions. An important feature of the cellular automaton algorithm is the consideration of the analytical exact solution for the grain boundary velocity, allowing tuning of parameters to ensure correct behavior of the algorithm. Following classical JMAK theory, the slope of Avrami plots of the recrystallized volume fraction should change from 2 to 3 as heterogeneous constant rate nucleation shifts

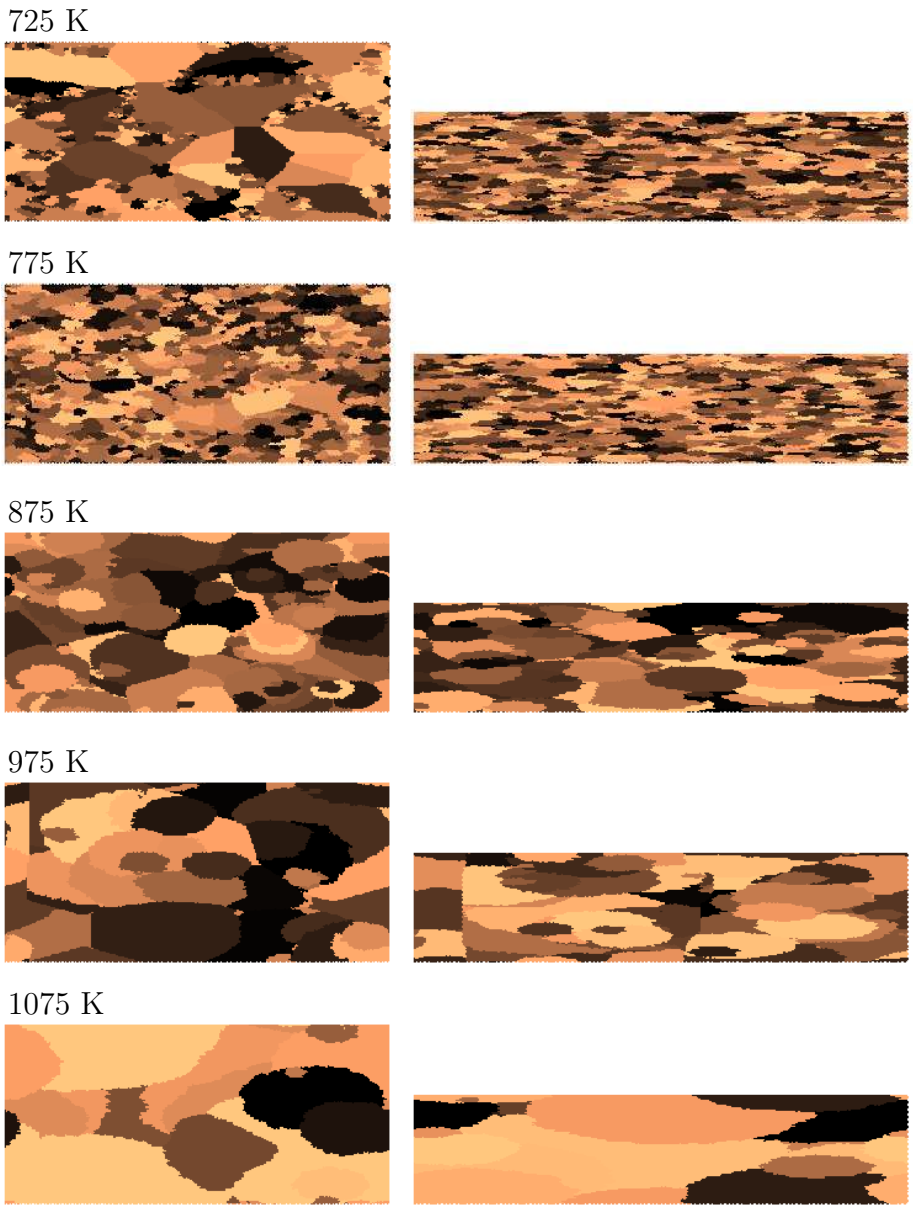

Figure 8: Microstructural evolution at five different and constant temperatures under deformation at a constant strain rate of 0.002 s^{-1}. The left and right columns show the microstructure at 50 and 100 % effective plastic strain, respectively. The coloring is randomly applied, just in order to distinguish between the different grains.

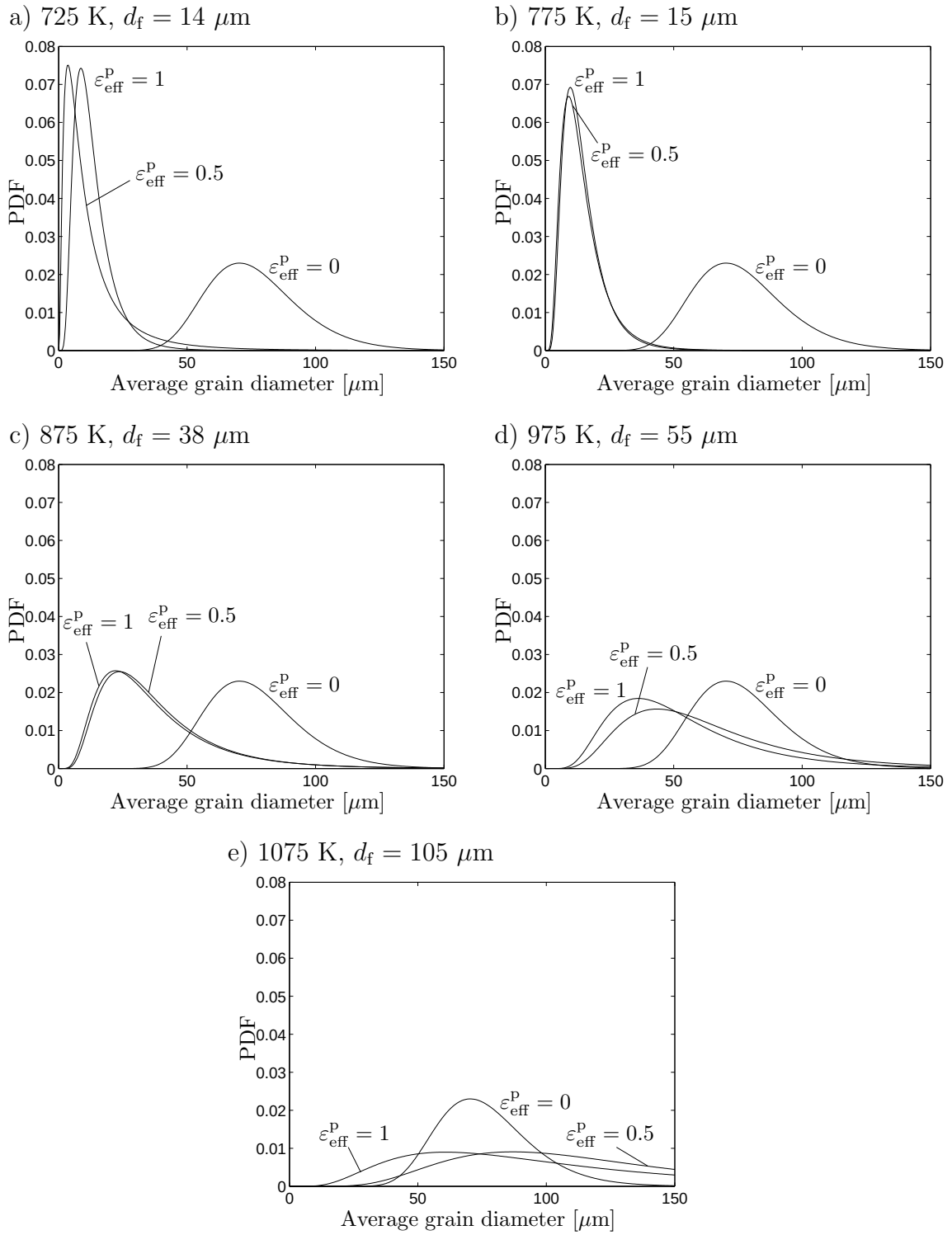

Figure 9: Probability density functions (PDF) for the grain size distribution at constant temperatures under deformation at a constant strain rate of 0.002 s^{-1}. The initial average grain size is 77 μm in all cases. The final grain size, d_f, is stated at each temperature.

towards site-saturated nucleation. This is shown to be captured by the present model as the nucleation rate is drastically increased – and thus tending towards site-saturation – as the temperature is reduced. In addition, tracing the strain state allows a post-processing step to be performed where the deformation of the material is imposed onto the analysis domain.

Calibration of the model parameters to pure Cu allows simulations to be performed of a hot compression process. The results replicate the expected nucleation of new grains along grain boundaries, giving a distinct necklace pattern. Following experimental evidence, this patterning effect is gradually lost as the temperature is increased and as larger saturation grain sizes are considered. The nuclei grow into equiaxed grains as predicted and with progressive plastic deformation a saturation grain size is reached where the average grain size obtained in simulations correspond well to experimental data. Flow stress curves based on the simulations exhibit the effects of cyclic recrystallization with the common transition from single-peak to multiple-peak serrated flow as the thermomechanical processing parameters are changed. Studying the effects of varied initial grain size, corresponding to having exposed the material to different heat treatment conditions, the macroscopic flow stress is influenced as expected. The extent of the flow stress serrations increases as the initial grain size is reduced while larger initial grain sizes stabilize the flow behavior, resulting in single-peak flow and a slower recrystallization process.

The proposed recrystallization model and cellular automaton formulation provide a versatile tool for studying the microstructural changes in a material during thermomechanical processing, where experimental results are replicated with good agreement by the simulations.

References

[1] R. D. Doherty, D. A. Hughes, F. J. Huphreys, J. J. Jonas, D. Juul Jensen, M. E. Kassner, W. E. King, T. R. McNelley, H. J. McQueen, and A. D. Rollett. Current issues in recrystallization: a review. *Materials Science and Engineering A*, 238:219–274, 1997.

[2] T. Sakai and J. J. Jonas. Dynamic recrystallization: Mechanical and microstructural considerations. *Acta Metallurgica*, 32(2):189–209, 1984.

[3] T. Sakai. Dynamic recrystallization microstructures under hot working conditions. *Journal of Materials Processing Technology*, 53:349–361, 1995.

[4] F. J. Humphreys and M. Hatherly. *Recrystallization and related annealing phenomena*. Pergamon, New York, second edition, 1996.

[5] W. Gao, A. Belyakov, H. Miura, and T. Sakai. Dynamic recrystallization of copper polycrystals with different purities. *Materials Science and Engineering*, A265:233–239, 1999.

[6] W. Roberts and B. Ahlbom. A nucleation criterion for dynamic recrystallization during hot working. *Acta Metallurgica*, 26:801–813, 1978.

[7] H. W. Hesselbarth and I. R. Göbel. Simulation of recrystallization by cellular automata. *Acta Metallurgica et Materialia*, 39(9):2135–2143, 1991.

[8] C. H. J. Davies. The effect of neighbourhood on the kinetics of a cellular automaton recrystallization model. *Scripta Metallurgica et Materialia*, 33(7):1139–1143, 1995.

[9] C. H. J. Davies. Growth of nuclei in a cellular automaton simulation of recrystallization. *Scripta Materialia*, 36(1):35–40, 1997.

[10] R. L. Goetz and V. Seetharaman. Modeling of dynamic recrystallization using cellular automata. *Scripta Materialia*, 38(3):405–413, 1998.

[11] D. Raabe. Cellular automata in materials science with particular reference to recrystallization simulation. *Annual Review of Materials Research*, 32:53–76, 2002.

[12] D. Raabe and L. Hantcherli. 2D cellular automaton simulation of the recrystallization texture of an IF sheet steel under consideration of Zener pinning. *Computational Materials Science*, 34:299–313, 2005.

[13] F. Lefevre-Schlick, Y. Brechet, H. S. Zurob, G. Purdy, and D. Embury. On the activation of recrystallization nucleation sites in Cu and Fe. *Materials Science and Engineering*, A502:70–78, 2009.

[14] Y. Estrin and H. Mecking. A unified phenomenological description of work hardening and creep based on one-parameter models. *Acta Metallurgica*, 32(1):57–70, 1984.

[15] H. S. Kim, Y. Estrin, E. Y. Gutmanas, and C. K. Rhee. A constitutive model for densification of metal compacts: the case of copper. *Materials Science and Engineering A*, 307:67–73, 2001.

[16] U. F. Kocks and H. Mecking. Physics and phenomenology of strain hardening: the FCC case. *Progress in Materials Science*, 48:171–273, 2003.

[17] H. Hallberg, M. Wallin, and M. Ristinmaa. Modeling of continuous dynamic recrystallization in commercial-purity aluminum. *Materials Science and Engineering*, A527:1126–1134, 2010.

[18] P. Peczak and M. J. Luton. The effect of nucleation models on dynamic recrystallization. I. Homogeneous stored energy distribution. *Philosophical Magazine B*, 68(1):115–144, 1993.

[19] P. Peczak and M. J. Luton. The effect of nucleation models on dynamic recrystallization. II. Heterogeneous stored-energy distribution. *Philosophical Magazine B*, 70(4):817–849, 1993.

[20] P. Peczak. A Monte Carlo study of influence of deformation temperature on dynamic recrystallization. *Acta Metallurgica et Materialia*, 43(3):1279–1291, 1995.

[21] R. Ding and Z. X. Guo. Coupled quantitative simulation of microstructural evolution and plastic flow during dynamic recrystallization. *Acta Materialia*, 49:3163–3175, 2001.

[22] C. Zheng, N. Xiao, D. Li, and Y. Li. Mesoscopic modeling of austenite static recrystallization in a low carbon steel using a coupled simulation method. *Computational Materials Science*, 45:568–575, 2009.

[23] J. E. Bailey and P. B. Hirsch. The recrystallization process in some polycrystalline metals. *Proceedings of the Royal Society of London, Series A*, 267(1328):11–30, April 1962.

[24] H. Xiao, H. Xie, Y. Yan, and J. Yanagimoto. Simulation of dynamic recrystallization using cellular automaton method. *Journal of the Iron and Steel Institute*, 11(2):42–45, March 2004.

[25] F. Chen, Z. Cui, J. Liu, X. Zhang, and W. Chen. Modeling and simulation on dynamic recrystallization of 30Cr2Ni4MoV rotor steel using the cellular automaton method. *Modelling and Simulation in Materials Science and Engineering*, 17:1–19, 2009.

[26] S. R. Chen and U. F. Kocks. On the strain-rate dependence of dynamic recrystallization in copper polycrystals. *Scripta Metallurgica et Materialia*, 27:1587–1592, 1992.

[27] J. E. Burke and D. Turnbull. Recrystallization and grain growth. *Progress in Metal Physics*, 3:220–292, 1952.

[28] F. J. Humphreys. A unified theory of recovery, recrystallization and grain growth, based on stability and growth of cellular microstructures - I. The basic model. *Acta Materialia*, 45(10):4231–4240, 1997.

[29] D. G. Cram, H. S. Zurob, Y. J. M. Brechet, and C. R. Hutchinson. Modelling discontinuous dynamic recrystallization using a physically based model for nucleation. *Acta Materialia*, 57:5218–5228, 2009.

[30] F. Montheillet, O. Lurdos, and G. Damamme. A grain scale approach for modeling steady-state discontinuous dynamic recrystallization. *Acta Materialia*, 57:1602–1612, 2009.

[31] S. Raghavan and S. S. Sahay. Modeling the grain growth kinetics by cellular automaton. *Materials Science and Engineering A*, 445-446:203–209, 2007.

[32] W. T. Read and W. Shockley. Dislocation models of crystal grain boundaries. *Physical Review*, 78:275–289, 1950.

[33] D. Wolf. A Read-Shockley model for high-angle grain boundaries. *Scripta Metallurgica*, 23:1713–1718, 1989.

[34] A. Mallick and S. Vedantam. Phase field study of the effect of grain boundary energy anisotropy on grain growth. *Computational Materials Science*, 46:21–25, 2009.

[35] D. Turnbull. Theory of grain boundary migration rates. *Journal of Metals, Transactions of the AIME*, 191(8):661–665, August 1951.

[36] H. S. Zurob, Y. Brechet, and J. Dunlop. Quantitative crietrion for recrystallization nucleation in single-phase alloys: Prediction of critical strains and incubation times. *Acta Materialia*, 54:3983–3990, 2006.

[37] R. E. Smallman and R. J. Bishop. *Modern Physical Metallurgy and Materials Engineering*. Butterworth-Heinemann, sixth edition, 1999.

[38] K. Kremeyer. Cellular automata investigations of binary solidifications. *Journal of Computational Physics*, 142:243–262, 1998.

[39] Y. J. Lan, D. Z. Li, and Y. Y. Li. A mesoscale cellular automaton model for curvature-driven grain growth. *Metallurgical and Materials Transactions*, 37B:119–129, 2006.

[40] N. Xiao, C. Zheng, D. Li, and Y. Li. A simulation of dynamic recrystallization by coupling a cellular automaton method with a topology deformation technique. *Computational Materials Science*, 41:366–374, 2008.

[41] D. Raabe and R. C. Becker. Coupling of a crystal plasticity finite-element model with a probabilistic cellular automaton for simulating primary static recrystallization in aluminium. *Modelling and Simulation in Materials Science and Engineering*, 8:445–462, 2000.

[42] T. Sakai and M. Ohashi. Dislocation substructures developed during dynamic recrystallization in polycrystalline nickel. *Materials Science and Technology*, 6:1251–1257, December 1990.

[43] H. Mecking and U. F. Kocks. Kinetics of flow and strain hardening. *Acta Metallurgica*, 29:1865–1875, 1981.

[44] N. A. Gjostein and F. N. Rhines. Absolute interfacial energies of [001] tilt and twist grain boundaries in copper. *Acta Metallurgica*, 7:319–330, May 1959.

[45] R. Viswanathan and C. Bauer. Kinetics of grain boundary migration in copper bicrystals with [001] rotation axes. *Acta Metallurgica*, 21(8):1099–1109, 1973.

[46] L. Blaz, T. Sakai, and J. J. Jonas. Effect of initial grain-size on dynamic recrystallization of copper. *Metal Science*, 17(12):609–616, 1983.

[47] A. M. Wusatowska-Sarnek, H. Miura, and T. Sakai. Nucleation and microtexture development under dynamic recrystallization of copper. *Materials Science and Engineering*, A323:177–186, 2002.

[48] M. Avrami. Kinetics of phase change, I. general theory. *Journal of Chemical Physics*, 7:1103–1112, December 1939.

[49] M. Avrami. Kinetics of phase change, II. Transformation-time relations for random distribution of nuclei. *Journal of Chemical Physics*, 8:212–224, February 1940.

[50] M. Avrami. Kinetics of phase change, III. Granulation, phase change and microstructure. *Journal of Chemical Physics*, 9:177–184, February 1941.

[51] A. D. Rollett, D. J. Srolowitz, R. D. Doherty, and M. P. Anderson. Computer simulation of recrystallization in non-uniformly deformed metals. *Acta Metallurgica*, 37(2):627–639, 1989.